Weak ferromagnetism in two-dimensional bilayered $Sr_{3-x}Ca_xRu_2O_7$

S. Ikeda
Department of Physics, Kyoto University, Kyoto 606-01, Japan
and Department of Physics, Hiroshima University, Higashi-Hiroshima 739, Japan

Y. Maeno
Department of Physics, Kyoto University, Kyoto 606-01, Japan

T. Fujita
Department of Physics, Hiroshima University, Higashi-Hiroshima 739, Japan

(Received 14 May 1997)

We have synthesized a bilayered ruthenate solid solution $Sr_{3-x}Ca_xRu_2O_7$ ($0 \leqslant x \leqslant 2.0$), which is homologous to the copper-free layered-perovskite superconductor Sr_2RuO_4 ($T_c = 1.5$ K). The x dependence of the lattice parameters, magnetic susceptibility $\chi(T)$, magnetization $M(H)$, and electrical resistivity $\rho(T)$ is systematically examined. Samples for all x show magnetic ordering below 150 K. It is shown, however, that the magnetic correlations change with increasing Ca content. The lowest ferromagnetic-ordering temperature in this series is observed at 3.2 K in the sample with $x(\mathrm{Ca}) = 1.0$. This transition is described well as a weakly ferromagnetic ordering by self-consistent renormalization (SCR) theory of spin fluctuations. To the best of our knowledge, this is the first example of applying the SCR theory to a weak ferromagnet with a quasi-two-dimensional layered crystal structure. [S0163-1829(98)00502-5]

I. INTRODUCTION

Discovery[1] of the superconductivity (SC) in Sr_2RuO_4 motivated us to search for other SC compounds among ruthenates and other $4d$-electron systems.[2] Recently, we have isolated[3] new ruthenate Mott insulators Ca_2RuO_4 in two structural phases. They are isostructural to Sr_2RuO_4 except for distortions present in Ca_2RuO_4. It is intriguing that Mott insulators are found in the vicinity of the superconductor not only for cuprates but also for ruthenates. In these ruthenates, strong electron-electron correlations appear to play a key role in determining their diverse properties.

A related ruthenate $Sr_3Ru_2O_7$, which has a tetragonal layered perovskite structure (Fig. 1), shows antiferromagneticlike ordering[4] below 15 K and nearly metallic behavior between 0.3 and 300 K. We regard $Sr_3Ru_2O_7$ as the next candidate for the ruthenate SC compound because of its two-dimensional RuO_2 bilayers and much lower magnetic ordering temperature than that of $SrRuO_3$ (the Curie temperature $T_c = 160$ K). In order to suppress the magnetic ordering, substitution of smaller Ca cations into Sr sites has been performed in $Sr_{3-x}Ca_xRu_2O_y$ (SCRO) with x up to 2.0. The synthesis of the series SCRO has already been reported in Ref. 5. Our previous study[2] suggested negative evidence for superconductivity in $Sr_2CaRu_2O_y$ ($x = 1.0$) down to 0.3 K. In this paper, we will show that a sharp change in the magnetic properties occurs at $x \approx 0.7$ and $x \approx 1.2$, accompanied by the change in the lattice parameters. We will also show that the magnetism around $x = 1.0$, where lowest magnetic ordering temperature is observed, is well described by means of the self-consistent renormalization theory of spin fluctuations.

Cao *et al.*[6,7] have reported remarkable magnetic and transport properties of the end members $Sr_3Ru_2O_7$ and $Ca_3Ru_2O_7$ using single crystals made by a flux method. They have concluded that the ground state of $Sr_3Ru_2O_7$ and $Ca_3Ru_2O_7$ are an itinerant ferromagnet and a nonmetal, respectively. Investigations using single crystals are of crucial importance especially in extracting the anisotropic properties and intrinsic transport properties. However, crystals grown by the flux method sometimes show significant differences in lattice parameters and physical properties from polycrystals, e.g., in (Sr,Ca)RuO_3 as described below. The origin of the discrepancies has not been understood at present, but the difference in stoichiometry or inclusion of impurity elements may play a crucial role. Therefore, we believe that the data obtained from polycrystals gives important complementary informa-

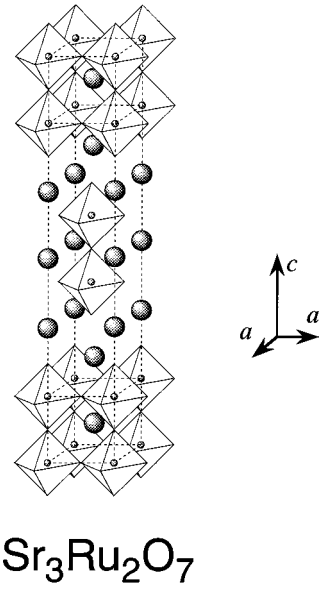

FIG. 1. The crystal structures of $Sr_3Ru_2O_7$. The large circle represents Sr and the small circle Ru. The cubes indicate RuO_6 octahedra.

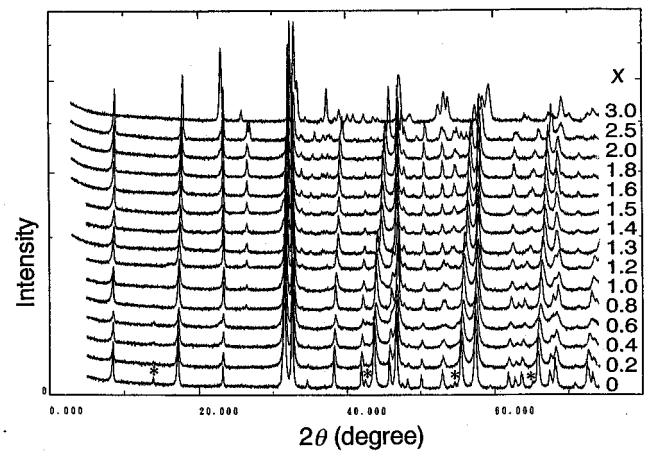

FIG. 2. X-ray powder-diffraction patterns of $Sr_{3-x}Ca_xRu_2O_y$ with varying Ca concentration x. All peaks of $0 \leqslant x \leqslant 2.0$ are consistent with the symmetry of $I4/mmm$. The asterisks indicate Sr_2RuO_4 impurity.

tion to those of the single crystals.

II. EXPERIMENT

We synthesized polycrystalline SCRO by a conventional solid-state reaction method. Stoichiometric mixtures of powders of $SrCO_3$ (99.99%), $CaCO_3$ (99.99%), and RuO_2 (99.9%) were ground and calcined in air for 24 h at 1173 K. The calcined samples were reground and pressed into pellets. They were then reacted and sintered in a flow of a weakly reducing gas mixture (99% Ar and 1% O_2) at 1473 K for 24 h and cooled in the furnace. The procedure was repeated at 1573 and 1623 K to obtain ''as-prepared'' samples. The reducing atmosphere is necessary to obtain SCRO phases. For example, firing the sample with $x(\mathrm{Ca})=1.5$ in a flow of 0.1 MPa O_2 at 1623 K results in decomposition into (Sr,Ca)O and unidentified phases. Some as-prepared samples were then oxidized by annealing at 773 K under oxygen atmosphere at relatively high pressure (1 and 5 MPa). For annealing at 773 K, ambient O_2 pressure was not adequate to prepare homogeneously oxidized samples because it resulted in the broadening of the peaks in the x-ray patterns, while 1 MPa O_2 annealing sustains the homogeneity of the samples.

The crystal structures of the samples at room temperature were characterized by powder x-ray diffraction. The oxygen content y was determined by the thermogravimetric analysis (TGA). The temperature dependence of magnetic susceptibility $\chi(T)$ from 2 to 350 K mostly under 1 T, the field dependence of magnetization $M(H)$ up to 5 T, and the ac magnetization with the frequency of 1 kHz and the amplitude of 0.1 mT were all measured by a superconducting quantum interference device magnetometer (Quantum Design, model MPMS-5S) using the sintered bar samples with the weight of 10–50 mg. The electrical resistivity $\rho(T)$ was measured by a standard four-terminal dc technique from 4.2 to 300 K. The specific heat C_P of $Sr_3Ru_2O_7$ was measured by the adiabatic heat pulse method from 1.2 to 25 K: the sample pellet with a diameter of 12 mm weighed about 2.5 g.

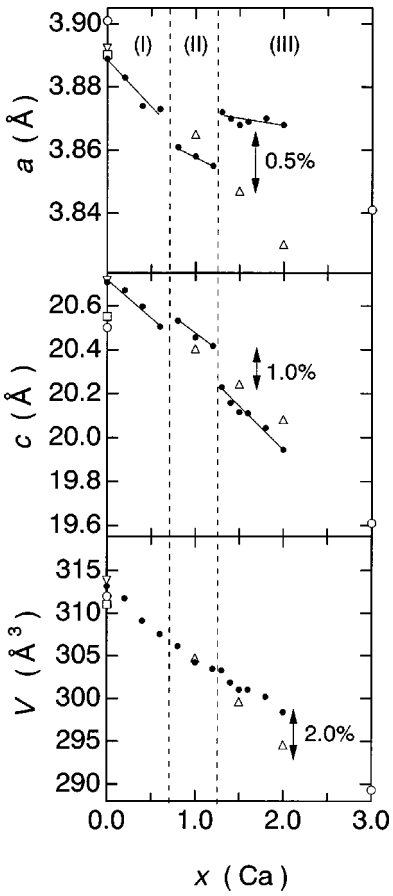

FIG. 3. The Ca concentration dependence of the a parameter, c parameter, and unit-cell volume. Closed circles indicate the as-prepared sample, open triangles indicate the oxidized sample (present work), open squares indicate single crystals [Müller-Buschbaum and Wilkens (Ref. 8)], inverted open triangle indicates polycrystals [Cava *et al.* (Ref. 4)], and open circles indicate single crystals [Cao *et al.* (Refs. 6,7)].

III. EXPERIMENTAL RESULTS

Powder x-ray diffraction spectra of as-prepared SCRO with different x(Ca) are shown in Fig. 2. The samples are essentially of single phase in the region $0 \leqslant x \leqslant 2.0$, although very weak impurity peaks of Sr_2RuO_4 are detected in the spectra of the samples with $0 \leqslant x \leqslant 0.6$. The spectra are well indexed in terms of the symmetry of tetragonal $I4/mmm$ group up to $x=2.0$. It is clear that the solubility range of Ca in $Sr_3Ru_2O_7$ is considerably wide although the ionic radius of divalent Ca is substantially smaller than that of Sr. Lattice parameters for both as-prepared and oxidized samples determined from the x-ray-diffraction spectra are plotted in Fig. 3. As we shall see below, three regions of distinct phases are clearly recognized: I($0 \leqslant x \leqslant 0.6$), II($0.6 < x \leqslant 1.2$), and III ($1.2 < x \leqslant 2.0$). Reflecting the smaller size of Ca ions, the unit-cell volume exhibits nearly linear contraction with increasing x for $0 \leqslant x \leqslant 2.0$. With increasing x, monotonic decrease in the c parameter is observed except in region II around $x=1.0$. The crystal structure in region II is characterized by an abrupt shortening of the a parameter by about 0.5% and stretching of the c parameter by about 1.0%. In Fig. 3, we also included the lattice parameters of single crystals and polycrystals reported by Müller-Buschbaum and

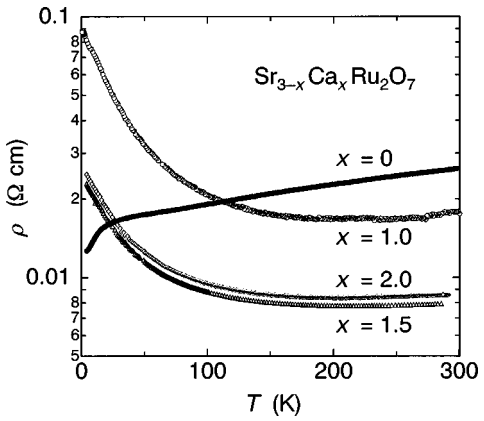

FIG. 4. Electrical resistivity between 4 and 300 K.

Wilkens,[8] Cao *et al.*[6,7] and Cava *et al.*,[4] respectively. It should be noted that between single crystals and polycrystals of $Sr_3Ru_2O_7$ there is a clear inconsistency in the lattice parameters, especially in the c parameter.

It is important for investigation of crystal structures and electronic configuration to determine the oxygen content. We decomposed powders of the as-prepared sample into SrO, CaO, and Ru by heating under the atmosphere of flowing Ar with 10% H_2 up to 1473 K at 2 K/min in a commercial TGA equipment. The results give the oxygen content y in $Sr_{3-x}Ca_xRu_2O_y$ to be 6.95 ± 0.06 for $x=0$, 6.99 ± 0.06 for $x=1.0$ and 7.01 ± 0.05 for $x=2.0$, indicating that y is essentially 7.0. This implies that the formal valency of the Ru ion remains tetravalent with four $4d$ electrons. Therefore the observed structural changes by Ca substitution are not driven by the change in oxygen content. Lattice distortions of $Sr_3Ru_2O_7$ have been examined by Inoue *et al.*[9] using transmission electron microscopy. They reported the evidence for rotation of the RuO_6 octahedra by about 1° around the c axis, with the direction of the rotation alternating from one layer to another within the bilayers. The existence of the rotation of the RuO_6 octahedra is in contrast with the absence of any lattice distortion in Sr_2RuO_4 down to low temperatures.[10,11] Oxidation effects on the lattice parameters are observed as shown in Fig. 3. For $x=1.5$, annealing in 1 MPa O_2 results in the increase in the c parameter by 0.63% and the decrease in the a parameter by 0.54%. The increase in the oxygen content Δy inferred from the sample weight is 0.25 ($y=7.25$). The excess oxygen atoms are probably positioned at interstitial sites within the rocksalt $(Sr,Ca)_2O_2$ layers. For $x=2.0$, the same tendency is observed. On the other hand, for $x=1.0$, the c parameter decreases by 0.45%, the a parameter slightly increases by 0.18% and $\Delta y=0.10$ ($y=7.10$) upon annealing in 5 MPa O_2 atmosphere. This behavior indicates that the oxidation effects in regions II and III are quite different. It is also remarkable that oxidation of samples in region III noticeably reduce the unit-cell volume, which is not seen in region II.

The electrical resistivities ρ of the as-prepared samples are shown in Fig. 4. Metallic temperature dependence is observed for $x=0$, and $d\rho/dT$ substantially increases below 15 K. Metallic temperature dependence is also observed for $x=1.0$, 1.5, and 2.0, although it changes to nonmetallic behavior at lower temperatures. Nevertheless, the measured values of ρ at 300 K are $\rho=8\sim30$ mΩ cm for $0\leqslant x\leqslant2.0$, at least three orders of magnitude lower in comparison with that of the insulator Sr_2IrO_4.[12,13] Therefore the nonmetallic behavior may be ascribed to grain-boundary resistance, and the intrinsic behavior may well be metallic to lower temperatures.

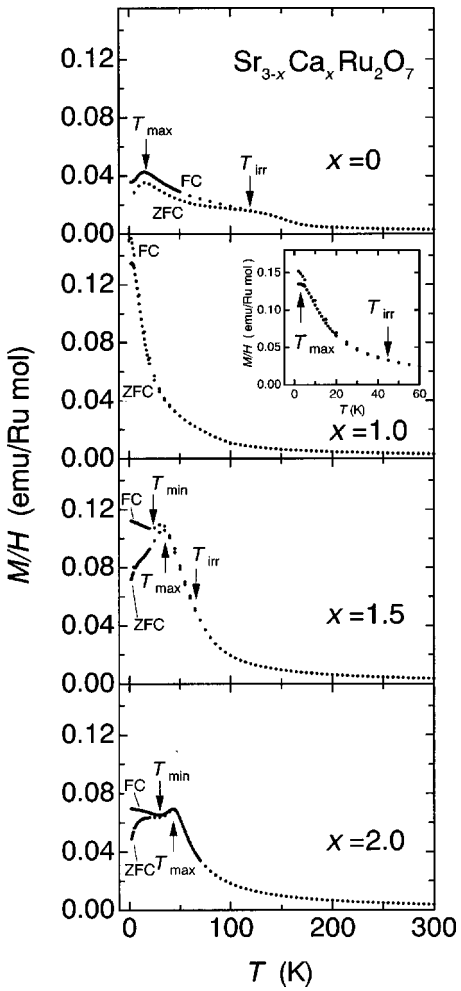

FIG. 5. Magnetic susceptibility under the field of 1 T. Both zero-field-cooling (ZFC) and field-cooling (FC) data are shown. Magnetic ordering temperature T_{max} is defined as the temperature where magnetic susceptibility takes a maximum value. See text for other notations.

The temperature dependence of the magnetic susceptibility $\chi(T)\equiv M/H$ under a field of 1 T, for both field-cooling (FC) and zero-field-cooling (ZFC) processes, is shown in Fig. 5. For $0\leqslant x\leqslant2.0$, $\chi(T)$ is fitted well with the Curie-Weiss behavior above 200 K and shows a cusp below 50 K. Magnetic ordering temperature T_{max} defined at maximum $\chi(T)$ varies with x as indicated by arrows in Fig. 5 and shown in the top frame of Fig. 6. In region I, T_{max} weakly increases with increasing x except at $x=0$. The samples in region I contain ferromagnetic impurity phase $(Sr,Ca)RuO_3$ ($T_c\leqslant160$ K) with the estimated amount about 1.6% from the magnetization measurements for $x=0$, although it is not detected in the x-ray spectra. In region II, T_{max} shows small values of 3–5 K and is nearly independent of x. Across the boundary ($x\approx1.2$) from region II to region III, T_{max} shows an abrupt increase. It increases up to 43 K ($x=2.0$) with further increasing x. The peak feature in the χ-T curve

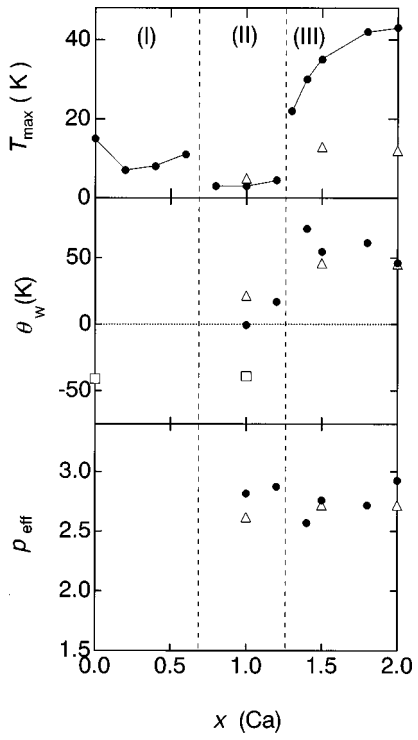

FIG. 6. The Ca concentration dependence of T_{max}, Weiss temperature θ_W, and the effective Bohr magneton p_{eff}. Closed circles indicate the as-prepared sample, open triangles indicate the oxidized sample, and open squares indicate θ_W obtained from the data between 300 and 700 K.

around T_{max} in region III is suppressed by a field of 5 T (Fig. 7), indicating that it is ascribed to weak antiferromagnetic ordering with small ferromagnetic components such as those induced by canted moments. Magnetization measurements under a weak magnetic field ($<10^{-3}$ T) indicated no sign of superconductivity above 2 K in all the as-prepared and oxidized samples.

We fitted the data of $\chi(T)$ between 200 and 350 K with $\chi(T)=\chi_0+\chi_{CW}$, where χ_0 is the temperature independent term and $\chi_{CW}=C/(T-\theta_W)$ is the temperature-dependent Curie-Weiss term. Here C is the Curie constant and θ_W is the Weiss temperature. The values of the effective Bohr magneton p_{eff} deduced from $C=N_A p_{eff}^2 \mu_B^2/3k_B$, where N_A is the

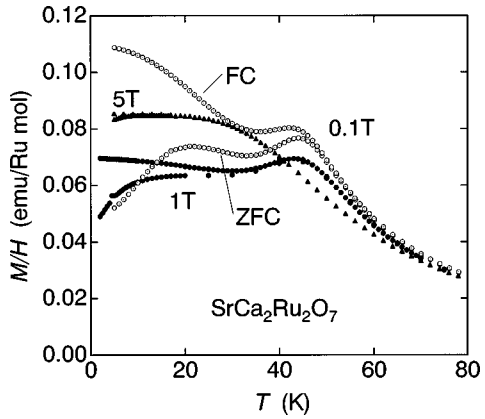

FIG. 7. Magnetic susceptibility of x(Ca)=2.0 under different fields. Both zero-field-cooling and field-cooling data are shown.

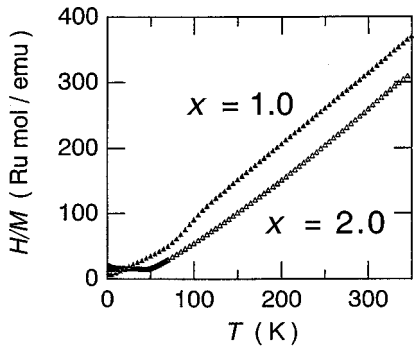

FIG. 8. The reciprocal magnetic susceptibility for $x=1.0$ and 2.0.

Avogadro number, μ_B is the Bohr magneton, and k_B is the Boltzmann constant, are shown in Fig. 6. We do not show p_{eff} and θ_W in region I because the data in region I clearly contain the contribution from the ferromagnetic impurity (Sr,Ca)RuO_3. Assuming that Ru^{4+} is in the low spin state in the tetragonal crystalline electric field $t_{2g}^4 e_g^0$ and that the orbital moment is quenched, we expect p_{eff} to be $g\{S(S+1)\}^{1/2}=2.83$, with $S=1$ and $g=2$. As shown in the bottom of Fig. 6, the observed effective Bohr magneton p_{eff} remains almost constant ($p_{eff}\sim 2.7$). This is consistent with the TGA results that the effective valence number of Ru ion in SCRO changes little by Ca substitution. On the other hand, the Weiss temperatures θ_W drastically change with increasing x from antiferromagnetic to ferromagnetic (Fig. 6). The inverse susceptibility χ^{-1} of samples with $x=1.0$ and 2.0 as a function of T shown in Fig. 8 clearly shows that the magnetic correlations of SCRO change with increasing Ca content. Because of the constancy of formal valence of Ru, we should rely on the information based on the structural modifications in order to clarify this drastic sign change of θ_W in this system. Since the a parameter is almost constant but the c parameter shrinks rapidly with increasing x except in region II, the change of magnetic correlations may have a relation to the change of the c parameter.

A similar variation of the magnetic correlation is well known in (Sr,Ca)RuO_3.[14] With substitution of Ca into $SrRuO_3$, magnetic correlations change from ferromagnetic to antiferromagnetic at $Sr_{0.4}Ca_{0.6}RuO_3$, despite the constancy of the formal Ru valency. In this three-dimensional system, only the compounds containing Sr shows ferromagnetic ordering, while no magnetic ordering occurs in compounds with antiferromagnetic Weiss temperatures such as $CaRuO_3$ and $LaRuO_3$.[15] Recent study of single crystalline (Sr,Ca)RuO_3 by Cao *et al.*[16] suggests that $Sr_{0.05}Ca_{0.95}RuO_3$, containing a very small amount of Sr, shows spin-glass-like ordering. It is noted that the corresponding polycrystalline samples do not yield any magnetic ordering. The origin of such discrepancies between single crystals grown by the flux method and polycrystalline samples should be clarified in future studies.

The temperature-independent χ_0 is estimated at about $\pm 10^{-4}$ emu/Ru mol. Taking a core diamagnetic contribution of about -8×10^{-5} emu/f.u. mol into account, we estimate the Pauli paramagnetic contribution χ_{Pauli} to be rather small and at most 2×10^{-4} emu/Ru mol. This contrasts with a large Pauli contribution of nearly 1×10^{-3} emu/Ru mol for

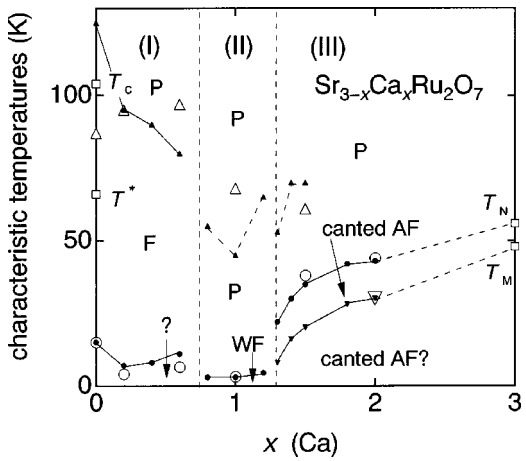

FIG. 9. T-x(Ca) phase diagram inferred from the results of dc and ac magnetization measurements. WF is the weakly ferromagnetic phase, P is the paramagnetic phase, F is the ferromagnetic phase, and AF is the antiferromagnetic phase. Closed circles indicate T_{max}, closed triangles indicate T_{irr}, inverted closed triangles indicate T_{min}, open circles indicate T_1', open triangles indicate T_2', inverted open triangles indicate T_3', and open squares indicate characteristic temperatures defined for single crystals (Refs. 6,7).

superconducting Sr_2RuO_4. Although Curie-Weiss analysis is not strictly valid for noninsulating compounds, the sign change of θ_W is obvious evidence for certain modifications of magnetic correlations in SCRO.

It is noted that the difference between FC and ZFC $\chi(T)$ is substantial in all regions, and especially strong in region I. To characterize the onset of this weak ferromagnetic ordering above T_{max} for $0 \leqslant x \leqslant 1.5$, we define T_{irr} as the temperature below which FC and ZFC exhibit irreversibility (Fig. 5). For $x \geqslant 1.8$ we could not detect such irreversibility above T_{max} within our experimental resolution. As we will show below, the ferromagnetism of SCRO below T_{irr} is clearly different from the contribution from (Sr,Ca)RuO_3. This implies that ferromagnetic components exist in SCRO. In Fig. 9, T_{irr} as well as T_{max} is shown as a function of x (T-x diagram). With increasing x, T_{irr} monotonically decreases in region I and the lowest value of T_{irr} is observed at $x=1.0$. In region III, a minimum in $\chi(T)$ below T_{max} is recognized for FC sequence as shown in Fig. 5. We therefore define yet another characteristic temperature T_{min} for this minimum, which shows a gradual increase with increasing x up to 2.0.

In order to detect T_{max}, T_{irr}, and T_{min} clearly, the real part of ac magnetization $M'(T)$ under almost zero field ($H_{dc} \leqslant 10^{-4}$ T and $H_{ac}=0.1$ mT) is displayed in Fig. 10. For all the Ca concentration there exist two characteristic peaks in $M'(T)$ at temperatures T_1' and T_2', or at T_1' and T_3', in addition to the ones ascribable to the ferromagnetic transition of the impurity (Sr,Ca)RuO_3. These temperatures are also plotted in the T-x diagram (Fig. 9) by open circles and triangles. It is clear that T_1' is identified with T_{max}. According to the reports by Cao *et al.*,[6,7] single crystalline $Sr_3Ru_2O_7$ ($Ca_3Ru_2O_7$) has two characteristic temperatures $T^*=66$ K and $T_c=104$ K ($T_M=48$ K and $T_N=56$ K). We also include these temperatures indicated by open squares in Fig. 9. For Sr-rich compounds, some inconsistencies of characteristic temperatures as well as lattice parameters are recognized between polycrystalline samples (our work and that of Cava

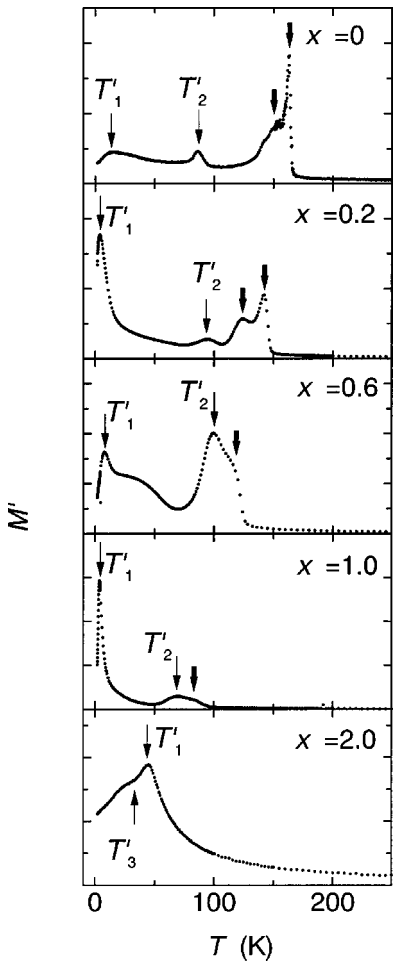

FIG. 10. The temperature dependence of ac susceptibility M' for different x from 2 to 200 K. Thick arrows indicate the peaks due to (Sr,Ca)RuO_3.

et al.[4]) and single crystals. In particular magnetic features at T_{max} and T_1' have not been recognized for single crystals. On the other hand, the data of single crystalline $Ca_3Ru_2O_7$ appears consistent with the extrapolation of the data of polycrystalline SCRO. The T-x diagram suggests that T_{irr} in region I corresponds to the T_c of single crystalline $Sr_3Ru_2O_7$,

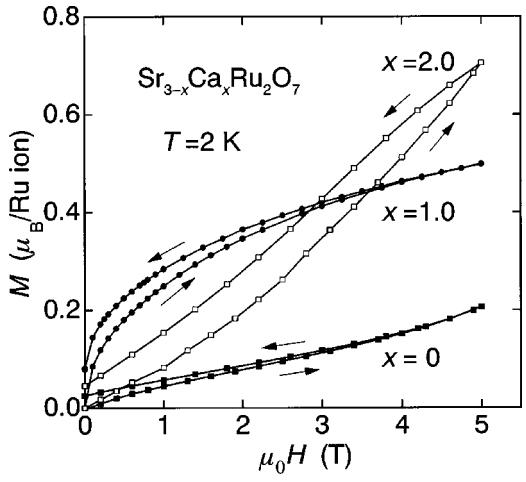

FIG. 11. The field dependence of magnetization at 2 K up to 5T.

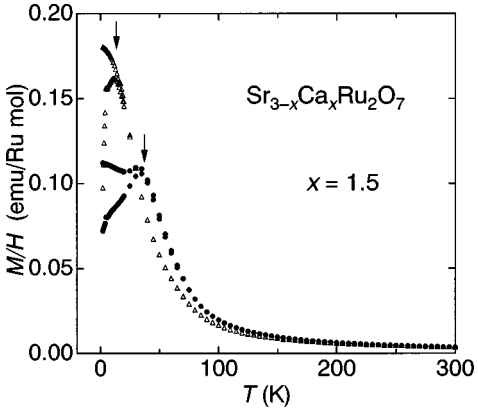

FIG. 12. Oxidation effects on $\chi(T) \equiv M/H$ for $x=1.5$. The magnetic ordering temperature T_{max} is diminished by O_2 annealing.

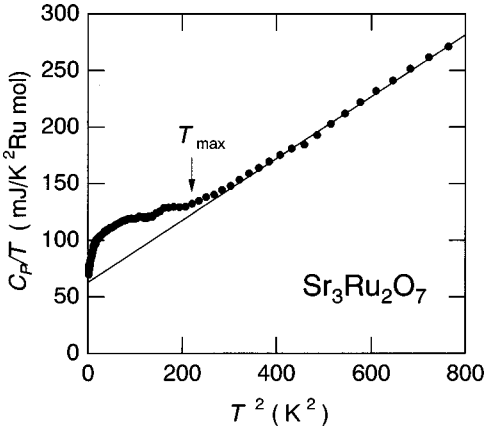

FIG. 13. Specific heat divided by temperature of $Sr_3Ru_2O_7$. Solid line represents the fitting $C/T=\gamma+\beta T^2$.

while T_{max} and T_{min} in region III to T_N and T_M, respectively, of single crystalline $Ca_3Ru_2O_7$. We will also discuss magnetic phases in T-x diagram later.

The nature of magnetism can be clarified from the field dependence of magnetization $M(H)$. Figure 11 shows $M(H)$ for the samples with different x at 2 K, below any magnetic ordering temperatures. It should be noted that the curvature of $M(H)$ for $x=1.0$ is quite different from those for $x=0$ and 2.0. With increasing applied field, $M(H)$ of $x=1.0$ reveals saturation behavior. On the other hand, such saturation is not observed in $M(H)$ of $x=0$ and 2.0, suggestive of metamagnetic transition at higher fields. $M(H)$ data of these three samples all show hysteresis behavior. The magnitude of the magnetic moment under a 5 T field increases with increasing x(Ca). This implies that the localized character of Ru-4d electrons in the ground state is enhanced in the Ca-rich phase, although its resistivity is metallic at high temperatures ($T>200$ K) and its magnetic moment is about four times smaller than that expected in the localized Heisenberg spin system.

Now we should consider the relation between structural instability and Ru-4d electron states. Increasing the content of smaller Ca leads to contraction of the unit-cell volume. By this contraction, stronger mixing between Ru-4d and O-2p electrons is naively expected. However, the results show the opposite tendency. The enhanced localized character may be due to the reduction in the overlap of wave functions of Ru-4d and O-2p which is caused by the distortion of RuO_6 octahedra with increasing x. This is analogous to the difference between metallic Sr_2RuO_4 and insulating Ca_2RuO_4.[3] In addition, by oxidation of the samples in region III, considered as the most distorted region, the c parameter increases, the a parameter decreases, and the temperature of the antiferromagneticlike transition at T_{max} is depressed as shown in Fig. 12. This indicates that the distortions of RuO_6 octahedra are released by interstitial oxygens and are important for antiferromagneticlike transition in region III. At low temperatures, spin reorientation is often associated with structural phase transitions. Recent structural study by Braden *et al.*[17] indicates that lattice distortions in orthorhombic Ca_2RuO_4 are described as the tiltings and rotations of rigid RuO_6 octahedra. In this SCRO system, structural refinements by neutron diffraction at low temperatures are needed to deepen the understanding of the ground state.

Specific heat divided by temperature C_P/T of $Sr_3Ru_2O_7$ is shown in Fig. 13. It is noted that no clear peak is observed around the magnetic ordering temperature at 15 K. Nevertheless, the T^2 dependence of C_P/T does not follow a linear relation of $C_P/T=\gamma+\beta T^2$ below 15 K. This may be due to a broad contribution of magnetic ordering to C_P. This broadening suggests that the magnetic ordering in $Sr_3Ru_2O_7$ is not three-dimensional but two-dimensional reflecting its crystal structure. In the range of temperature between 400 $K^2 \leqslant T^2 \leqslant 800$ K^2, fitting the data using the formula above gives the Sommerfeld coefficient of $\gamma=63$ mJ/Ru mol K^2 and $\beta=0.273$ mJ/Ru mol K^4. The Debye temperature is evaluated as $\theta_D=350$ K from $\beta=12\pi^4 N k_B/5\theta_D^3$ where $N=6$ is the number of atoms in formula unit. The largest specific-heat γ value of $Sr_3Ru_2O_7$ among the Sr-Ru-O Ruddelsden-Popper phases [30 mJ/Ru mol K^2 for $SrRuO_3$ (Ref. 18) and 38 mJ/Ru mol K^2 for Sr_2RuO_4 (Refs. 19,20)] provides clear evidence that $Sr_3Ru_2O_7$ is a strongly correlated 4d electron metallic oxide. A local-density electronic-band-structure calculation has been performed for $Sr_3Ru_2O_7$ by Hase and Nishihara.[21] They deduced the density of states $D(E_F)=10.3$ states/eV cell and electronic specific-heat coefficient $\gamma_{band}=12.1$ mJ/Ru mol K^2. Thus the mass enhancement factor $\gamma_{exp}/\gamma_{band}=5.2$ surpasses that of Sr_2RuO_4 at $\gamma_{exp}/\gamma_{band}=3.6$.[19,22] It is necessary to measure C_P for other concentrations x in the SCRO system in order to elucidate whether the ground state is metallic or not.

IV. DISCUSSIONS

A. The SCR analysis for $Sr_2CaRu_2O_7$

The SCRO system shows both the Curie-Weiss behavior of magnetic susceptibility and noninsulating electrical resistivity. Similar properties were observed in the mixed metallic phase (Sr,Ca)RuO_3 and were discussed in terms of the self-consistent renormalization theory (SCR theory[23]) as an itinerant ferromagnet.[24] The SCR theory of spin fluctuations for a weak ferromagnet should be appropriate for analyzing the magnetism in SCRO, especially in region II where very low T_{max} (3–5 K) is observed. The Arrott plot of magnetization curves for $x=1.0$ at different temperatures is shown in Fig. 14. The appearance of the positive intercept on the vertical

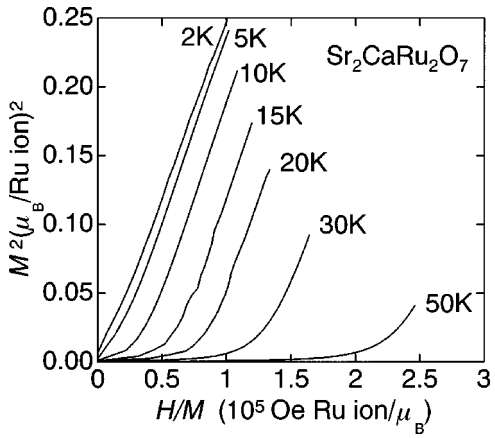

FIG. 14. Arrott plot of $M(H)$ data with $x=1.0$ at different temperatures.

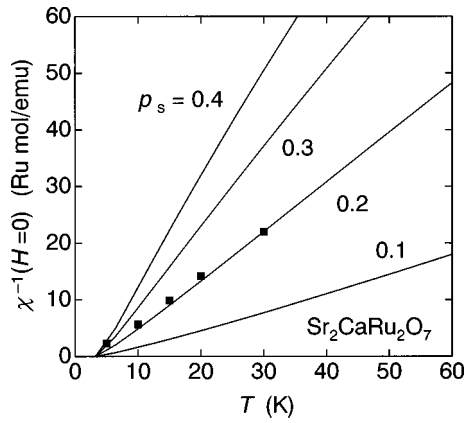

FIG. 15. Results of $\chi(T,H=0)^{-1}$ calculated for $x=1.0$ by means of SCR theory. It depends on parameters $\overline{F_1}$, T_c, T_0, and T_A in addition to p_S. Several different values for p_S are assumed and $p_S=0.2$ gives the best fit as shown.

axis indicates that the intrinsic Curie temperature T_c is below 5 K. Therefore we regard $T_{max}=3.2$ K, not $T_{irr}=45$ K, as the intrinsic Curie temperature T_c. Only the data in region II satisfy the relation that M^2 is proportional to H/M. The spontaneous magnetization per one magnetic ion $p_S \geqslant M/\mu_B(H=0)=0.08$ at 2 K is much smaller than the effective Bohr magneton $p_{eff}=2.82$ evaluated from $\chi(T)$. These characterize SCRO in region II as a weak ferromagnet.

For itinerant electron systems, magnetic anisotropy is not substantial in comparison with localized electron systems, since magnetic correlation length is considerably longer than the cell dimensions. For region II, the low Curie temperature of $\sim 10^0$ K indicates that magnetic anisotropy energy is evaluated at most $10^{-2}-10^{-1}$ K. Thus the observed magnetization $M(H)$ up to 5 T (Fig. 14) for the polycrystalline samples should reflect the intrinsic process. Nevertheless, a recent theory by Hatatani and Moriya[25] discusses a subtle difference in the behavior of the isotropic two-dimensional system of spin fluctuations from that of the isotropic three-dimensional system.

In weakly ferromagnetic metals, the SCR theory gives the relation:

$$\frac{p_S^2}{4}=\frac{15T_0}{T_A}\,c\left(\frac{T_c}{T_0}\right)^{4/3}, \tag{1}$$

where $c=0.33536$ is a constant, T_c is the Curie temperature, and T_0 and T_A characterize the energy width of the dynamical spin-fluctuation spectrum and the width of the distribution of the static susceptibility in the **q** space, respectively. T_0 and T_A correspond to the exchange energy J in the localized spin system. A much larger ratio of T_A/T_c than unity means that spin fluctuations only near $\mathbf{q}=0$ contribute to the magnetic ordering.

We consider the relation derived by Takahashi:[26]

$$\overline{F_1}=\frac{4k_BT_A^2}{15T_0}, \tag{2}$$

where $\overline{F_1}$ is the fourth-order expansion coefficient of the magnetic free energy which depends on M. $\overline{F_1}$ can be derived from the gradient of the Arrott plot as

$$\frac{16\mu_B}{\overline{F_1}}\frac{H}{M}=M(H)^2-M(0)^2, \tag{3}$$

where H and M are expressed in Oe and μ_B/Ru ion, respectively.

It is not appropriate to estimate the spontaneous magnetization p_S ($T=0$ K) from the data of $M(H)$ at 2 K because this temperature cannot be regarded as much below $T_c=3.2$ K. Therefore, we regard p_S as a fitting parameter and fit the inverse magnetic susceptibility in the limit of zero field, $\chi^{-1}(T,H=0)$, using the following relations in order to determine the SCR parameters as in Ref. 27. Assuming the weakly ferromagnetic limit, i.e., $T_c/T_0 \ll 1$, the relations are simplified as follows:

$$y=\frac{\overline{F_1}p_S^2}{8T_A\eta^2}\left\{-1+\frac{1+\nu y}{c}\int_0^{1/\eta}dz\cdot z^3\left[\ln u-\frac{1}{2u}-\Psi(u)\right]\right\}, \tag{4}$$

with

$$y=\frac{N_A}{2T_A\chi\eta^2}, \tag{5}$$

$$\eta=\left(\frac{T_c}{T_0}\right)^{1/3}, \tag{6}$$

$$\nu=\frac{\eta^2T_A}{U}, \tag{7}$$

$$u=\frac{z(y+z^2)}{t}, \tag{8}$$

where $\Psi(u)$ is the digamma function, U is the intra-atomic exchange energy, and $t=T/T_c$. Using these relations and assuming $U=10^4$ K, we can predict $\chi(T,H=0)$ above T_c for several values of p_S as shown in Fig. 15. For experimental $\chi(T,H=0)$ we employ positive intercepts in the Arrott plot (Fig. 14) where the line of extrapolation of high-field data crosses the horizontal axis. Adequate reproduction of $\chi(T,H=0)$ is obtained when p_S is 0.2. Furthermore, T_0 and

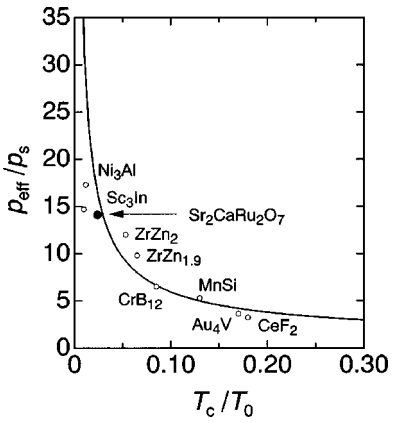

FIG. 16. Generalized Rhodes-Wohlfarth plots after Takahashi (Ref. 26). The data of $Sr_2CaRu_2O_7$ is shown by a solid circle. The solid line is the theoretical expectation.

T_A are evaluated self-consistently from Eqs. (1), (2), and (4). All the SCR parameters thus evaluated are, $T_c=3.2$ K, $p_S=0.2$, $\overline{F_1}=433$ K, $T_0=133$ K, and $T_A=465$ K.

The ratios $T_c/T_0=0.024$ and $p_{eff}/p_S=14.1$ are important for the classification of the itinerant/localized ferromagnets. Figure 16 is based on the generalized Rhodes-Wohlfarth plot (p_{eff}/p_S vs T_c/T_0) for weak ferromagnets by Takahashi.[26] In this plot, large p_{eff}/p_S and small T_c/T_0 represents the strong itinerant character of electrons. The localized Heisenberg system is characterized by $p_{eff}/p_S=T_c/T_0=1$. $Sr_2CaRu_2O_7$ ($x=1.0$) is regarded as a weakly ferromagnetic metal with intermediate character as shown. For polycrystalline $Sr_{0.4}Ca_{0.6}RuO_3$, Kiyama *et al.*[24] obtained $T_c=25$ K and $T_A\approx5000$ K from $M(H)$, thus $T_A/T_c\approx200$. The almost identical value of $T_A/T_c=145$ for $Sr_2CaRu_2O_7$ indicates that the weak ferromagnetism in both compounds is quite similar despite the difference in dimensionality of the Ru-O network. Our study is, to our knowledge, the first example of applying the SCR theory to a ferromagnet with a quasi-two-dimensional layered crystal structure.[25] Theoretical calculations of Takahashi's relation [Eq. (2)] for a quasi-two-dimensional system should be required in order to advance the investigation of the quasi-two-dimensional weak ferromagnet. Nevertheless it is expected that the analysis presented here remains qualitatively valid also for systems with quasi-two-dimensional ferromagnetic spin fluctuations.[28]

B. Phase diagram

In this section, we summarize the structural and magnetic phase diagram of $Sr_{3-x}Ca_xRu_2O_7$. Three regions I, II, and III are well distinguished by the lattice parameters and magnetic ordering temperatures. For each region, there exist two or three characteristic temperatures as observed in the magnetization measurements. We give the interpretation of these temperatures below.

In region I, the paramagnetic phase changes to ferromagnetic at T_{irr}. There exists another phase below T_{max}. However, it is not clear from the present study what type of magnetism the ground state has. In region II, T_{max} is the Curie temperature characterized by itinerant weak ferromagnetism. T_{irr} is not essential for magnetism because the Arrott plot clearly shows that a spontaneous moment appears only below T_{max}. In region III, T_{max} is an antiferromagnetic transition temperature with canted ferromagnetism. According to the result of $Ca_3Ru_2O_7$ by Cao *et al.*,[7] T_{min} may correspond to spin-reorientation temperature to greater canting. It is difficult to determine whether T_{irr} observed in this region is intrinsic or not. Ultimately, we can make the magnetic phase diagram of SCRO already shown in Fig. 9. Structural study below characteristic temperatures of each phase will help confirming the interpretation given here.

Next, we discuss the distinction between three phases I, II, and III. As analyzed in Sec. IV A, region II is well described by the itinerant weak ferromagnetism and is quite different from the others. This difference is also consistent with the singularity of the x dependence of the lattice parameters. The expectation of the metamagnetic transition above a field of 5 T in regions I and III suggests that the magnetic ground state in these regions is rather localized than that in region II. As already described, region III is more localized than region I, corresponding to enhanced lattice distortion. As a result, the magnetic ground states of the $Sr_{3-x}Ca_xRu_2O_7$ system are characterized by the changeover from the itinerant weak ferromagnetism to the localized spin system with increasing x.

Especially in region I, the discrepancies between polycrystalline and single-crystalline samples are recognized in the lattice parameters and magnetism. Future investigations with single crystals grown by a different method may help clarify this issue.[29]

V. CONCLUSION

In summary, we have characterized the magnetic and structural properties of the bilayered ruthenate series $Sr_{3-x}Ca_xRu_2O_y$ ($0\leqslant x\leqslant 2.0$). The oxygen content y has been determined as essentially 7.0 for all x before annealing oxidizing atmosphere. With increasing Ca, the magnetic correlations of SCRO change dramatically and the localized character in the ground state is enhanced for high Ca concentration. The magnetic properties in the region around $x=1.0$ are associated with the appearance of weak ferromagnetism. On the basis of the SCR parameters $Sr_2CaRu_2O_7$ is classified as the weak ferromagnet with a quasi-two-dimensional crystal structure.

ACKNOWLEDGMENTS

We are grateful to K. Yoshimura, T. Kiyama, T. Moriya, and Y. Takahashi for their useful advice in analyzing the data using the SCR theory. We thank I. Hase for discussing his band-structure calculation results prior to publication. We thank Y. Koyama, Y. Inoue, M. Hara, S. Nakatsuji, G. Cao, M. Braden, and Y. Morii for valuable discussions and greatly acknowledge T. Ishiguro for his support. We also thank H. Muranishi, K. Yoshida, and S. Nishizaki for their technical support. Y.M. is supported by a grant from Kawasaki Steel 21st Century Foundation. Some of the measurements were performed at the Cryogenic Center of Hiroshima University.

[1] Y. Maeno, H. Hashimoto, K. Yoshida, S. Nishizaki, T. Fujita, J. G. Bednorz, and F. Lichtenberg, Nature (London) **372**, 532 (1994).
[2] S. Ikeda, Y. Maeno, M. Nohara, and T. Fujita, Physica C **263**, 558 (1996).
[3] S. Nakatsuji, S. Ikeda, and Y. Maeno, J. Phys. Soc. Jpn. **66**, 1868 (1997).
[4] R. J. Cava, H. W. Zandbergen, J. J. Krajewski, W. F. Peck, Jr., B. Batlogg, S. Carter, R. M. Fleming, O. Zhou, and L. W. Rupp, Jr., J. Solid State Chem. **116**, 141 (1995).
[5] S. Ikeda, Y. Maeno, H. Muranishi, and T. Fujita, J. Low Temp. Phys. **105**, 1599 (1996).
[6] G. Cao, S. McCall, and J. E. Crow, Phys. Rev. B **55**, R672 (1997).
[7] G. Cao, S. McCall, J. E. Crow, and R. P. Guertin, Phys. Rev. Lett. **78**, 1751 (1997).
[8] Hk. Müller-Buschbaum and J. Wilkens, Z. Anorg. Allg. Chem. **591**, 161 (1990).
[9] Y. Inoue, M. Hara, Y. Koyama, S. Ikeda, Y. Maeno, and T. Fujita, in *Advances in Superconductivity IX*, edited by S. Nakajima and M. Murakami (Springer-Verlag, Tokyo, 1997), p. 281.
[10] J. S. Gardner, G. Balakrishnan, D. McK. Paul, and C. Haworth, Physica C **265**, 251 (1996).
[11] M. Braden, A. H. Moudden, S. Nishizaki, Y. Maeno, and T. Fujita, Physica C **273**, 248 (1997).
[12] M. K. Crawford, M. A. Subramanian, R. L. Harlow, J. A. Fernandez-Baca, Z. R. Wang, and D. C. Johnston, Phys. Rev. B **49**, 9198 (1994).
[13] M. Itoh, T. Shimura, Y. Inaguma, and Y. Morii, J. Solid State Chem. **118**, 206 (1995).
[14] A. Kanbayashi, J. Phys. Soc. Jpn. **44**, 108 (1978).
[15] R. J. Bouchard, and J. F. Weiher, J. Solid State Chem. **4**, 80 (1972).
[16] G. Cao, S. McCall, M. Shepard, J. E. Crow, and R. P. Guertin, Phys. Rev. B **56**, 321 (1997).
[17] M. Braden *et al.* (private communication).
[18] P. B. Allen, H. Berger, O. Chauvet, L. Forro, T. Jarlborg, A. Junod, B. Revaz, and G. Santi, Phys. Rev. B **53**, 4393 (1996).
[19] Y. Maeno, K. Yoshida, H. Hashimoto, S. Nishizaki, S. Ikeda, M. Nohara, T. Fujita, A. P. Mackenzie, N. E. Hussey, J. G. Bednorz, and F. Lichtenberg, J. Phys. Soc. Jpn. **66**, 1405 (1997).
[20] A. P. Mackenzie, S. Ikeda, Y. Maeno, T. Fujita, S. R. Julian, and G. G. Lonzarich (unpublished).
[21] I. Hase and Y. Nishihara, J. Phys. Soc. Jpn. **66**, 3517 (1997).
[22] T. Oguchi, Phys. Rev. B **51**, 1385 (1995).
[23] T. Moriya, *Spin Fluctuations in Itinerant-Electron Magnetism* (Springer-Verlag, Berlin, 1985).
[24] T. Kiyama, K. Yoshimura, and K. Kosuge, in *Advances in Superconductivity IX* (Ref. 9), p. 171.
[25] M. Hatatani and T. Moriya, J. Phys. Soc. Jpn. **64**, 3434 (1995).
[26] Y. Takahashi, J. Phys. Soc. Jpn. **55**, 3553 (1986).
[27] Y. Takahashi and T. Moriya, J. Phys. Soc. Jpn. **54**, 1592 (1985).
[28] Y. Takahashi, J. Phys. Condens Matter **9**, 10 359 (1997).
[29] G. Cao, S. C. McCall, J. E. Crow, and R. P. Guertin, Phys. Rev. B **56**, 5387 (1997).